


Topological properties of multilayers and surface steps in the SnTe material class

Wojciech Brzezicki , Marcin M. Wysockiński, and Timo Hyart

International Research Centre MagTop, Institute of Physics, Polish Academy of Sciences, Aleja Lotnikow 32/46, PL-02668 Warsaw, Poland

 (Received 14 December 2018; revised manuscript received 29 March 2019; published 16 September 2019)

Surfaces of multilayer semiconductors typically have regions of atomically flat terraces separated by atom-high steps. Here we investigate the properties of the low-energy states appearing at the surface atomic steps in $\text{Sn}_{1-x}\text{Pb}_x\text{Te}_{1-y}\text{Se}_y$. We identify the important approximate symmetries and use them to construct relevant topological invariants. We calculate the dependence of mirror- and spin-resolved Chern numbers on the number of layers and show that the step states appear when these invariants are different on the two sides of the step. Moreover, we find that a particle-hole symmetry can protect one-dimensional Weyl points at the steps. Since the local density of states is large at the step the system is susceptible to different types of instabilities, and we consider an easy-axis magnetization as one realistic possibility. We show that magnetic domain walls support low-energy bound states because the regions with opposite magnetization are topologically distinct in the presence of nonsymmorphic chiral and mirror symmetries, providing a possible explanation for the zero-bias conductance peak observed in the recent experiment [Mazur *et al.*, *Phys. Rev. B* **100**, 041408(R) (2019)].

DOI: [10.1103/PhysRevB.100.121107](https://doi.org/10.1103/PhysRevB.100.121107)

$\text{Sn}_{1-x}\text{Pb}_x\text{Te}_{1-y}\text{Se}_y$ systems have attracted interest due to the realization of a three-dimensional topological crystalline insulator phase [1–5], prediction of two-dimensional (2D) topological phases [6–10], and the appearance of low-energy states at the defects [11,12]. Robust one-dimensional (1D) modes were observed at the surface steps separating regions of even and odd number of layers [12] and interpreted as topological flat bands using a model obeying a chiral symmetry [13]. In a more accurate description step modes can have a band width but the local density of states (LDOS) is large so that the system is susceptible to the formation of correlated states [11,14,15]. Recent experiments indicate that an order parameter emerges at low temperatures and it is accompanied with an appearance of a robust zero-bias peak (ZBCP) in the tunneling conductance [16,17]. The temperature and magnetic field dependence of the energy gap are consistent with superconductivity and under such circumstances the ZBCP is often interpreted as an indication of Majorana zero modes [16–19], which are intensively searched non-Abelian quasiparticles [20]. Thus, this finding calls for a critical study of different mechanisms which may explain the appearance of the ZBCP.

We show that $\text{Sn}_{1-x}\text{Pb}_x\text{Te}_{1-y}\text{Se}_y$ multilayers are a paradigmatic system for realization of topological phases due to emergent symmetries of the low-energy theory, and ZBCP can appear in the absence of superconductivity. The important 2D topological invariants are the mirror-resolved Chern number C_{\pm} (due to structural mirror symmetry) and spin-resolved Chern number $C_{\uparrow(\downarrow)}$ (due to approximate spin-rotation symmetry). For odd number of layers N the mirror symmetry is a point-group operation whereas for even N it is a nonsymmorphic (NS) symmetry (Fig. 1), so that adding one layer can change the topology of the system [9,10]. We calculate the dependence of the Chern numbers on N and show that the step states appear when these invariants are different on the two sides of the step. The theory and experiment [12,13] attribute step states only to odd-height steps, but we predict

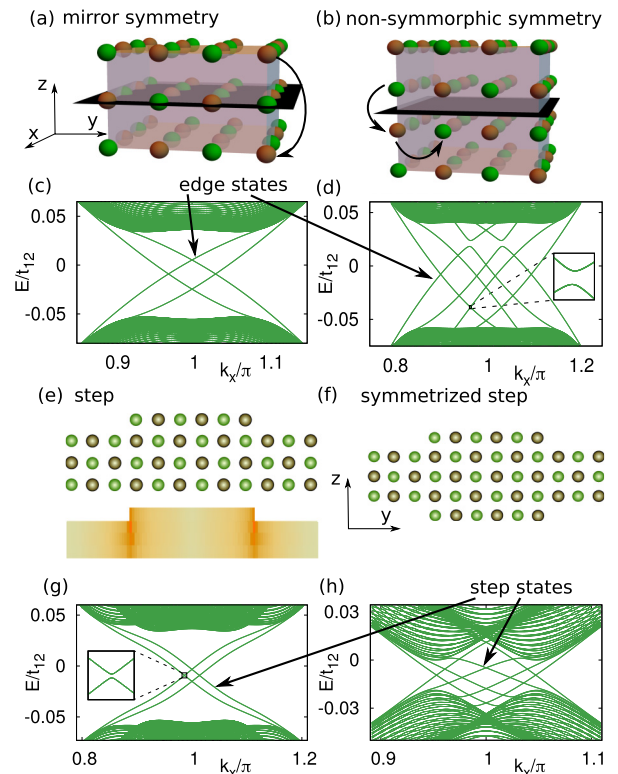


FIG. 1. (a),(b) Schematic views of the $\text{Sn}_{1-x}\text{Pb}_x\text{Te}_{1-y}\text{Se}_y$ multilayers stacked in the (001) direction. Green (brown) balls are (Sn,Pb) [(Te,Se)] atoms. For odd (even) number of layers N there exists symmorphic (nonsymmorphic) mirror symmetry. (c),(d) The corresponding edge-state spectra for $N = 3$ and $N = 4$. (e) Surface atomic steps describing an interface between three- and four-layer systems and (f) a symmetrized atomic step. (g),(h) The corresponding spectra for step modes. The panel below (e) shows local density of states of the step states. The width of the sample is $N_y = 600$.

that also even-height steps can exhibit step states consistent with another experiment [21].

We discuss the conditions under which a spontaneous symmetry breaking gives rise to an energy gap at the step and study an easy-axis magnetic order as one possibility. We show that magnetic domain walls (DWs) support low-energy bound states because the regions with opposite magnetization are topologically distinct in the presence of NS chiral and mirror symmetries. Due to the appearance of DWs the Fermi level is pinned to the energy of the DW states for a range of electron density providing an explanation for the ZBCP observed in the experiment [16]. The observed temperature and magnetic field dependencies are consistent with our theory.

Our starting point is a p -orbital tight-binding Hamiltonian describing a bulk topological crystalline insulator in the $\text{Sn}_{1-x}\text{Pb}_x\text{Te}_{1-y}\text{Se}_y$ -material class [1]:

$$\begin{aligned} \mathcal{H}(\mathbf{k}) = & m\mathbb{1}_2 \otimes \mathbb{1}_3 \otimes \Sigma + t_{12} \sum_{\alpha=x,y,z} \mathbb{1}_2 \otimes (\mathbb{1}_3 - L_\alpha^2) \otimes h_\alpha^{(1)}(k_\alpha) \\ & + t_{11} \sum_{\alpha \neq \beta} \mathbb{1}_2 \otimes \left[\mathbb{1}_3 - \frac{1}{2}(L_\alpha + \varepsilon_{\alpha\beta} L_\beta)^2 \right] \otimes h_{\alpha,\beta}^{(2)}(k_\alpha, k_\beta) \Sigma \\ & + \sum_{\alpha=x,y,z} \lambda_\alpha \sigma_\alpha \otimes L_\alpha \otimes \mathbb{1}_8, \end{aligned} \quad (1)$$

where we have chosen a cubic unit cell with internal sites at the corners labeled by $i = 1, \dots, 8$ [22], $\varepsilon_{\alpha\beta}$ is a Levi-Civita symbol, $L_\alpha = -i\varepsilon_{\alpha\beta\gamma}$ are the 3×3 angular momentum $L = 1$ matrices, σ_α are Pauli matrices acting in the spin space, Σ is a diagonal 8×8 matrix with entries $s_i = \pm 1$ at the two sublattices [(Sn,Pb)/(Te,Se) atoms], and $h_\alpha^{(1)}(k_\alpha)$ and $h_{\alpha,\beta}^{(2)}(k_\alpha, k_\beta)$ are 8×8 matrices describing hopping between the nearest-neighbor and next-nearest-neighbor lattice sites in the directions $\hat{\alpha}$ and $\hat{\alpha} + \varepsilon_{\alpha\beta}\hat{\beta}$, respectively [22]. We allow the possibility to tune the spin-orbit coupling terms λ_α ($\alpha = x, y, z$) to be different from each other although in the real material $\lambda_\alpha = \lambda$. When not otherwise stated we use $m = 1.65$ eV, $t_{12} = 0.9$ eV, $t_{11} = 0.5$ eV, and $\lambda = 0.3$ eV [23].

We focus on Hamiltonian $\mathcal{H}_N(\vec{k})$ for N layers in the z direction. The mirror symmetries for odd (even) N can be written as $M_z^{o/e}(k_x) = \sigma_z \otimes (2L_z^2 - 1) \otimes m_z^{o/e}(k_x)$, where m_z^o is a point-group reflection and $m_z^e(k_x)$ is a (momentum-dependent) NS operation consisting of reflection and a shift by a half lattice vector [Figs. 1(a) and 1(b)]. To calculate C_\pm we split $\mathcal{H}_N(\vec{k})$ into two blocks in the $M_z^{o/e}(k_x)$ eigenspace. Since $M_z^{o/e}(k_x)$ anticommutes with time-reversal symmetry (TRS) operator $\mathcal{T} = K\sigma_y \otimes \mathbb{1}_3 \otimes \mathbb{1}_8$, these blocks carry opposite Chern numbers C_\pm [24]. We find that C_+ oscillates between $+2$ and -2 for $N = 2n + 1$ (we exclude $N = 1$) and $C_\pm = 0$ for $N = 2n$ ($n \in \mathbb{N}$) [22,25]. We point out that for even number of layers the nonsymmorphic nature of the mirror symmetry guarantees that the Chern number calculated for the blocks must always be equal to zero. Therefore, one can equivalently conclude that the mirror-resolved Chern number does not exist as a topological invariant for even number of layers. The edge-state spectra for $N = 3$ and $N = 4$ are shown in Figs. 1(c) and 1(d). As predicted by $C_\pm = \mp 2$ we see two pairs of gapless edge modes in the case $N = 3$, but surprisingly we

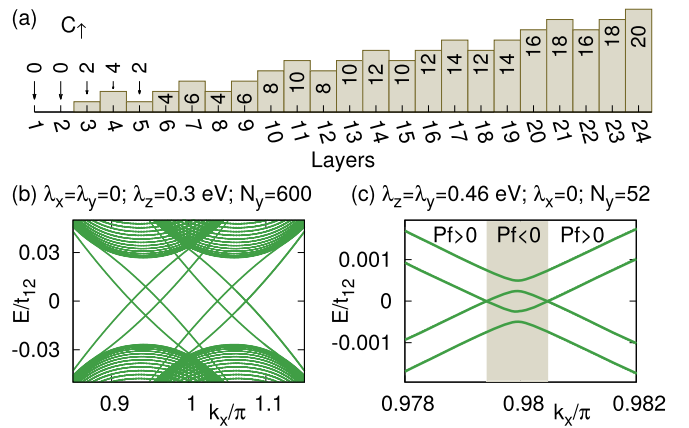


FIG. 2. (a) Spin-resolved Chern numbers C_\uparrow as a function of N for $\lambda_x = \lambda_y = 0$. Because we have switched off λ_x and λ_y the effective spin-orbit coupling becomes smaller. In the case of odd number of layers where C_\pm is a useful topological invariant, we have checked that this reduction of the spin-orbit coupling does not change the C_\pm so that it is reasonable to use $\lambda_z = 0.3$ eV. The only exception is the case $N = 3$ where we have used renormalized $\lambda_z = 0.5$ eV to keep C_\pm fixed. (b) The spectrum for $N = 4$ showing gapless edge modes. (c) Gapless spectrum for a step between $N = 3$ and $N = 4$ can be protected by a \mathbb{Z}_2 invariant if $\lambda_x = 0$.

find four pairs of edge modes if $N = 4$. These edge modes are consistent with $C_\pm = 0$ because there exist small gaps which do not vanish by increasing system size.

To understand the existence of edge modes in the case of $N = 4$ we notice that the momentum in the z direction is quantized and the low-energy degrees of freedom are associated with a motion within the (x, y) plane [26]. Therefore, the components of the spin-orbit coupling λ_α ($\alpha = x, y, z$) contribute differently to the spectrum, and the dominant effect comes from $\lambda_z \sigma_z L_z$. Hence, turning off λ_x and λ_y is a good approximation [cf. Figs. 1(d) and 2(b)] and this leads to a spin rotation symmetry with respect to the z axis. Thus, by block-diagonalizing $\mathcal{H}_N(\vec{k})$ we can calculate $C_\uparrow = -C_\downarrow$ as a function of N [22]. The results are shown in Fig. 2(a) and suggest that C_\uparrow grows linearly with N and takes values $C_\uparrow = 2 + 4m$ ($m \in \mathbb{Z}$) for odd N and $C_\uparrow = 4m$ ($m \in \mathbb{Z}$) for even N . The careful study of whether this behavior persists for arbitrary thickness goes beyond the scope of the current Rapid Communication, but importantly this numerical evidence is already enough that we obtain a topological description of step modes for reasonably large systems, including all the systems considered in this Rapid Communication. In particular, the result for $N = 4$ is consistent with the number of edge modes in Figs. 1(d) and 2(b). For $\lambda_x = \lambda_y = 0$ the tiny gaps originally present in the spectrum vanish completely.

These Chern numbers provide an interpretation for the appearance of the step modes because they appear whenever C_\uparrow is different on the two sides of the step [Figs. 1(e)–1(h)] [22]. For a step separating even N and odd N $\Delta C_\uparrow = 2 + 4m$ ($m \in \mathbb{Z}$) and therefore at least two pairs of helical step modes [27] exist at these steps in agreement with Refs. [12,13] [Figs. 1(e) and 1(g)]. These step modes are weakly gapped because the spin-rotation symmetry is only present as an approximate symmetry. However, we can use C_\pm to show that

these gaps vanish in the limit $N \rightarrow \infty$. Namely, by using a symmetrized step construction shown in Figs. 1(f) and 1(h) and fixing N so that $C_+ = \pm 2$ on the different sides of the step, we find that in a system containing steps on both surfaces there exist $|\Delta C_+| = 4$ pairs of gapless edge modes protected by the mirror symmetry. In the limit $N \rightarrow \infty$ the step modes at the different surfaces are completely decoupled, and therefore each step supports two pairs of gapless edge modes. Interestingly, we find that (depending on N) also even-height steps can exhibit $|\Delta C_+| = 4$ or $|\Delta C_+| = 4|m|$ ($m \in \mathbb{Z}$) pairs of step modes consistent with the experiment [21].

In the case of a one-atom-high step and finite N the step modes are weakly gapped even though C_\pm are different on two sides of the step because the step breaks the mirror symmetry and hybridizes the mirror blocks. However, the step modes can still be exactly gapless for certain widths N_y in the y direction if $\lambda_x = 0$ [Fig. 2(c)]. This effect comes from the existence of an effective particle-hole symmetry which together with a mirror symmetry gives rise to an antiunitary chiral symmetry $\mathcal{S} = \mathcal{K}\sigma_y \otimes (2L_x^2 - 1) \otimes (i\Sigma m_x)$, where m_x is a mirror reflection with respect to the x plane interchanging the sublattices [22]. Due to this symmetry the Hamiltonian $\mathcal{H}_{N,N_y}(k_x)$ supports a \mathbb{Z}_2 Pfaffian invariant, which protects a 1D Weyl point if it changes sign as a function of k_x [28,29]. As demonstrated in Fig. 2(c) this kind Weyl points can be realized at the steps if $\lambda_x = 0$.

Since we have now established the topological origin of the step modes in the noninteracting system, we turn our attention to the correlation effects (e.g., spin, charge, orbital, or superconducting order), which are inevitably present due to the large LDOS in the limit $N \gg 1$ [11,14,15,22]. Our aim is to show that there exists a mechanism for the appearance of the ZBCP in the absence of superconductivity (without analyzing the competition between different types of order [22]). We require that the order parameter opens an energy gap, which means that it breaks the symmetries associated with $C_{\uparrow(\downarrow)}$ and C_\pm . Thus, we assume that there exists a magnetic instability in the vicinity of the steps (due to magnetic impurities or electron-electron interactions [22]) giving rise to a Zeeman field $H_Z = \mathbf{h} \cdot \vec{\sigma}$. Because the step modes are approximately spin polarized along the z direction the directions of \mathbf{h} within the (x, y) plane are efficient in opening an energy gap, and due to spin-orbit coupling the gap depends on the direction of \mathbf{h} within the (x, y) plane [22]. Therefore, the system realizes an easy-axis ferromagnet and the topological defects are DWs [30]. In the following we consider $\mathbf{h} = (h_x, 0, 0)$.

To study the topological DW states we determine the low-energy theory for a single step, the emergent symmetries, and the topological invariants. Although h_x breaks TRS the spectrum of a system with two steps still exhibits Kramers degeneracy at $k_x = \pi$ [Fig. 1(g)] due to a remaining NS TRS $\mathcal{T}'(k_x) = \mathcal{K}\mathbb{1}_2 \otimes (2L_y^2 - 1) \otimes g(k_x)r_z$, where $g(k_x)$ is a diagonal matrix with entries $e^{\pm ik_x/2}$ and r_z denotes π rotation with respect to the z axis [22]. $\mathcal{T}'(k_x)$ squares to $+1$ (-1) at $k_x = 0$ ($k_x = \pi$) which yields Kramers degeneracy only at $k_x = \pi$. We assign half of the states at $k_x = \pi$ to each step by selecting from each Kramers' doublet the state with larger projection on each step. Our low-energy theory is obtained by expanding the Hamiltonian around $k_x = \pi$ in one of the subspaces of the

projected states [22]. By assuming $\lambda_y = 0$ the system supports a k -dependent mirror symmetry $M_x(k_x) = \sigma_x \otimes (2L_x^2 - 1) \otimes g(k_x)$ and NS chiral symmetry $S(k_x) = i\sigma_y \otimes \mathbb{1}_3 \otimes \Sigma m_x g(k_x)$ [Fig. 3(a)] [22].

We find that in the presence of these symmetries there exist three topologically distinct phases shown in Fig. 3(b). The trivial phase for $|h_x| < h_c$ is separated from the two nontrivial ones by the energy gap closings at $h_x = \pm h_c$. The nontrivial phases are characterized by a NS chiral \mathbb{Z}_2 invariant $\nu = 1$ [22,31], and the phases at $h_x < -h_c$ and $h_x > h_c$ are topologically distinct because the band inversions occur in the different mirror sectors $M_x(\pi) = \pm 1$ [Fig. 3(b)]. It is not *a priori* known whether the DWs between the topologically distinct phases in this symmetry class support DW states [31]. However, our calculations show that sharp interfaces between trivial and nontrivial phases (two nontrivial phases) support one (two) low-energy bound state(s) per DW [Figs. 3(c)–3(f)]. The number of low-energy states in each case is consistent with the number of zero-energy DW states expected in the case of smooth DWs with slowly varying spin textures [22]. Although these states resemble the zero-energy DW states considered in the context of a Dirac equation [32] and the Su-Schrieffer-Heeger (SSH) model [33–35], there is an important difference because they are realized in a model belonging to a different symmetry class. Namely, the appearance of the DW breaks the symmetries, and therefore the energies of these states in the case of sharp DWs remain nonzero even if the DWs are well separated [22]. Moreover, the energies depend on the tight-binding parameters and in this sense they resemble the topological DW states in systems with more complicated unit cells consisting of three or more atoms [36]. Nevertheless, for realistic system parameters the DW states appear close to the zero energy [22].

Because the DW states have nonzero energy, in high-resolution tunneling spectroscopy one would observe two split peaks in the conductance. However, already small broadening of the energy levels leads to a single ZBCP [Figs. 3(g) and 3(h)] [22]. Moreover, for sufficiently large density of DWs the bound states hybridize and form a band inside the energy gap leading to a single ZBCP where the height of the peak depends on the density of DWs [Figs. 3(e) and 3(h)]. The ZBCP is robust against variations of the density because in analogy to the SSH model [35] we expect that the DWs are the lowest-energy charged excitations in the system, and therefore small density of excess electrons (excess holes) is accommodated in the system by increasing the number of DWs, so that up to a critical variation of the density the Fermi level is pinned to the energy of the DW states. A similar situation occurs in quantum Hall ferromagnets where the lowest-energy charged excitations are skyrmions [37] which appear due to excess electrons and have been observed experimentally [38]. Also the parametric dependencies of the ZBCP and the energy gap are consistent with the experiment [16]. The increase of temperature suppresses the order parameter and the energy gap. The external magnetic field breaks the degeneracy of states with opposite magnetization leading to a confinement between the DWs similarly as a symmetry-breaking term in the SSH model [35], so that the number of DWs and the magnitude of the ZBCP decrease.

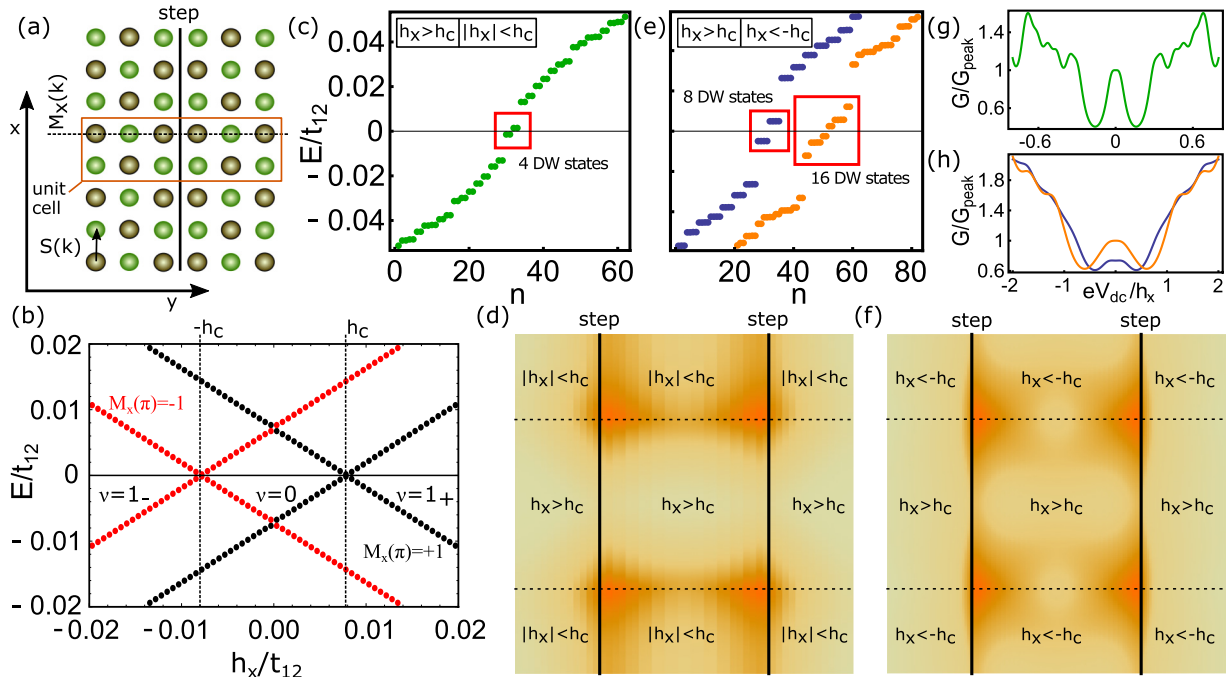


FIG. 3. (a) Schematic representation of symmetries $M_x(k_x)$ and $S(k_x)$ operating at a single step [22]. (b) The energies of the step states at $k_x = \pi$ as a function of h_x for $N_y = 52$ and $\lambda_z = \lambda_x = 0.5$ eV. The states are colored according to the eigenvalues of $M_x(\pi)$. There exist three topologically distinct phases denoted as trivial phase $\nu = 0$ and nontrivial phases with $\nu = 1_{\pm}$. The nontrivial phases are distinct from the trivial phase due to NS chiral \mathbb{Z}_2 invariant ν [22,31]. The lower index ± 1 describes the subspace of $M_x(\pi) = \pm 1$ where the band inversion occurs. (c),(d) Spectrum and LDOS for a system with DWs separating trivial and nontrivial phases. The system supports four low-energy bound states at the four DWs. The parameters are $N_x = 260$, $N_y = 52$, and $\lambda_z = \lambda_x = 0.5$ eV. In the trivial (nontrivial) phase $h_x = 0.003$ eV ($h_x = 0.04$ eV). (e),(f) Same for a system with DWs separating two nontrivial phases with opposite magnetizations. The system supports eight low-energy bound states at the four DWs [orange dots in (e)]. If the number of DWs is increased to eight there exist 16 low-energy bound states [orange dots in (e)]. The parameters are $N_x = 160$, $N_y = 140$, $|h_x| = 0.034$ eV, $\lambda_z = 0.5$ eV, and $\lambda_x = 0$. (g),(h) The differential conductance G as a function of bias voltage V_{dc} [22] corresponding to spectra in (c) and (e), respectively. In all figures $\lambda_y = 0$. The magnitude of the gap and h_x in our simulations are larger than in the experiment by Mazur *et al.* [16], but they necessarily decrease for larger N because the bulk gap decreases and the dispersion of the step states gets flatter [22].

Furthermore, we find that by increasing the Zeeman field the energy gap of the system decreases [22]. Therefore, all the observations can be explained without requiring the existence of superconductivity. Finally, the observation that magnetic dopants enhance the ZBCP and the energy gap [16] makes it more plausible that the effect originates from magnetic instability instead of superconductivity. The systematic analysis of the correlated states which are consistent with the observations [16] and the exploration of the possible common origin of the zero-bias anomalies in various topological semi-

conductors and semimetals [16–19] are interesting directions for future research [22].

We thank T. Dietl, J. Tworzydło, Ł. Skowronek, G. Mazur, M. Cuoco, R. Rechciński, and R. Buczko for discussions. The work is supported by the Foundation for Polish Science through the IRA Programme cofinanced by EU within the SG OP Programme. W.B. also acknowledges support by Narodowe Centrum Nauki (NCN, National Science Centre, Poland) Project No. 2016/23/B/ST3/00839.

[1] T. H. Hsieh, H. Lin, J. Liu, W. Duan, A. Bansil, and L. Fu, Topological crystalline insulators in the SnTe material class, *Nat. Commun.* **3**, 982 (2012).
 [2] P. Dziawa, B. J. Kowalski, K. Dybko, R. Buczko, A. Szczerbakow, M. Szot, E. Lusakowska, T. Balasubramanian, B. M. Wojek, M. H. Berntsen, O. Tjernberg, and T. Story, Topological crystalline insulator states in $\text{Pb}_{1-x}\text{Sn}_x\text{Se}$, *Nat. Mater.* **11**, 1023 (2012).
 [3] Y. Tanaka, Z. Ren, T. Sato, K. Nakayama, S. Souma, T. Takahashi, K. Segawa, and Y. Ando, Experimental realization of a topological crystalline insulator in SnTe, *Nat. Phys.* **8**, 800 (2012).

[4] S.-Y. Xu, C. Liu, N. Alidoust, M. Neupane, D. Qian, I. Belopolski, J. D. Denlinger, Y. J. Wang, H. Lin, L. A. Wray, G. Landolt, B. Slomski, J. H. Dil, A. Marcinkova, E. Morosan, Q. Gibson, R. Sankar, F. C. Chou, R. J. Cava, A. Bansil, and M. Z. Hasan, Observation of a topological crystalline insulator phase and topological phase transition in $\text{Pb}_{1-x}\text{Sn}_x\text{Te}$, *Nat. Commun.* **3**, 1192 (2012).
 [5] L. Fu, Topological Crystalline Insulators, *Phys. Rev. Lett.* **106**, 106802 (2011).
 [6] J. Liu and L. Fu, Electrically tunable quantum spin Hall state in topological crystalline insulator thin films, *Phys. Rev. B* **91**, 081407(R) (2015).

- [7] S. Safaei, M. Galicka, P. Kacman, and R. Buczko, Quantum spin Hall effect in IV-VI topological crystalline insulators, *New J. Phys.* **17**, 063041 (2015).
- [8] J. Liu, T. H. Hsieh, P. Wei, W. Duan, J. Moodera, and L. Fu, Spin-filtered edge states with an electrically tunable gap in a two-dimensional topological crystalline insulator, *Nat. Mater.* **13**, 178 (2014).
- [9] D. Bassanezi, E. O. Wrasse, and T. M. Schmidt, Symmetry-dependent topological phase transitions in PbTe layers, *Mater. Res. Express* **5**, 015051 (2018).
- [10] A. L. Araújo, G. J. Ferreira, and T. M. Schmidt, Suppressed topological phase transitions due to nonsymmorphism in SnTe stacking, *Sci. Rep.* **8**, 9452 (2018).
- [11] E. Tang and L. Fu, Strain-induced partially flat band, helical snake states and interface superconductivity in topological crystalline insulators, *Nat. Phys.* **10**, 964 (2014).
- [12] P. Sessi, D. Di Sante, A. Szczerbakow, F. Glott, S. Wilfert, H. Schmidt, T. Bathon, P. Dziawa, M. Greiter, T. Neupert, G. Sangiovanni, T. Story, R. Thomale, and M. Bode, Robust spin-polarized midgap states at step edges of topological crystalline insulators, *Science* **354**, 1269 (2016).
- [13] R. Rechciński and R. Buczko, Topological states on uneven (Pb,Sn)Se (001) surfaces, *Phys. Rev. B* **98**, 245302 (2018).
- [14] G. E. Volovik, Graphite, graphene, and the flat band superconductivity, *JETP Lett.* **107**, 516 (2018).
- [15] R. Ojajärvi, T. Hyart, M. A. Silaev, and T. T. Heikkilä, Competition of electron-phonon mediated superconductivity and Stoner magnetism on a flat band, *Phys. Rev. B* **98**, 054515 (2018).
- [16] G. P. Mazur, K. Dybko, A. Szczerbakow, J. Z. Domagala, A. Kazakov, M. Zgirski, E. Lusakowska, S. Kret, J. Korczak, T. Story, M. Sawicki, and T. Dietl, Experimental search for the origin of zero-energy modes in topological materials, *Phys. Rev. B* **100**, 041408(R) (2019).
- [17] S. Das, L. Aggarwal, S. Roychowdhury, M. Aslam, S. Gayen, K. Biswas, and G. Sheet, Unexpected superconductivity at nanoscale junctions made on the topological crystalline insulator $\text{Pb}_{0.6}\text{Sn}_{0.4}\text{Te}$, *Appl. Phys. Lett.* **109**, 132601 (2016).
- [18] H. Wang, H. Wang, H. Liu, H. Lu, W. Yang, S. Jia, X.-J. Liu, X. C. Xie, J. Wei, and J. Wang, Observation of superconductivity induced by a point contact on 3D Dirac semimetal Cd_3As_2 crystals, *Nat. Mater.* **15**, 38 (2016).
- [19] L. Aggarwal, A. Gaurav, G. S. Thakur, Z. Haque, A. K. Ganguli, and G. Sheet, Unconventional superconductivity at mesoscopic point contacts on the 3D Dirac semimetal Cd_3As_2 , *Nat. Mater.* **15**, 32 (2016).
- [20] R. M. Lutchyn, E. P. A. M. Bakkers, L. P. Kouwenhoven, P. Krogstrup, C. M. Marcus, and Y. Oreg, Majorana zero modes in superconductor–semiconductor heterostructures, *Nat. Rev. Mater.* **3**, 52 (2018).
- [21] D. Iaia, C. Y. Wang, Y. Maximenko, D. Walkup, R. Sankar, F. Chou, Y. M. Lu, and V. Madhavan, Topological nature of step edge states on the surface of topological crystalline insulator $\text{Pb}_{0.7}\text{Sn}_{0.3}\text{Se}$, *Phys. Rev. B* **99**, 155116 (2019).
- [22] See Supplemental Material at <http://link.aps.org/supplemental/10.1103/PhysRevB.100.121107> for more details, which includes Refs. [39–61].
- [23] For small systems the tight-binding parameters can deviate significantly from the bulk values and lead to different topological properties [10]. However, we consider small systems only for illustration purposes. Our results are based on symmetry and topological considerations which are valid for sufficiently large systems ($\gtrsim 10$ layers) where the bulk values of the parameters can be used.
- [24] C.-K. Chiu, J. C. Y. Teo, A. P. Schnyder, and S. Ryu, Classification of topological quantum matter with symmetries, *Rev. Mod. Phys.* **88**, 035005 (2016).
- [25] For $N = 2n$ the $M_z^e(k_x)$ eigenspace depends on $k_x/2$. Thus the Hamiltonian blocks become 4π -periodic in k_x and they have additional TRS with respect to the point $\vec{k}^* = (-\pi, 0)$, so that $C_{\pm} = 0$ [22].
- [26] Notice that this reasoning is valid also if the states are localized in the vicinity of the surface in the z direction even if the system itself is infinite.
- [27] Due to bulk-boundary correspondence there will be $|\Delta C_{\uparrow}|$ step modes with spin \uparrow propagating in one direction and $|\Delta C_{\downarrow}| = |\Delta C_{\uparrow}|$ step modes with spin \downarrow propagating in the opposite direction.
- [28] Y. X. Zhao, A. P. Schnyder, and Z. D. Wang, Unified Theory of PT and CP Invariant Topological Metals and Nodal Superconductors, *Phys. Rev. Lett.* **116**, 156402 (2016).
- [29] W. Brzezicki and M. Cuoco, Topological gapless phases in nonsymmorphic antiferromagnets, *Phys. Rev. B* **95**, 155108 (2017).
- [30] Also other types of order parameters can naturally support the appearance of domain walls, and the magnetic order is considered here only as an example.
- [31] K. Shiozaki, M. Sato, and K. Gomi, Z_2 topology in nonsymmorphic crystalline insulators: Möbius twist in surface states, *Phys. Rev. B* **91**, 155120 (2015).
- [32] R. Jackiw and C. Rebbi, Solitons with fermion number 1/2, *Phys. Rev. D* **13**, 3398 (1976).
- [33] W. P. Su, J. R. Schrieffer, and A. J. Heeger, Solitons in Polyacetylene, *Phys. Rev. Lett.* **42**, 1698 (1979).
- [34] W. P. Su, J. R. Schrieffer, and A. J. Heeger, Soliton excitations in polyacetylene, *Phys. Rev. B* **22**, 2099 (1980).
- [35] A. J. Heeger, S. Kivelson, J. R. Schrieffer, and W. P. Su, Solitons in conducting polymers, *Rev. Mod. Phys.* **60**, 781 (1988).
- [36] M. Nurul Huda, S. Kezilebieke, T. Ojanen, R. Drost, and P. Liljeroth, Tuneable topological domain wall states in engineered atomic chains, [arXiv:1806.08614](https://arxiv.org/abs/1806.08614).
- [37] S. M. Girvin, The quantum Hall effect: Novel excitations and broken symmetries, in *Topological Aspects of Low Dimensional Systems*, edited by A. Comtet, T. Jolicoeur, S. Ouvry, and F. David (Springer-Verlag, Berlin and Les Editions de Physique, Les Ulis, 2000).
- [38] S. E. Barrett, G. Dabbagh, L. N. Pfeiffer, K. W. West, and R. Tycko, Optically Pumped NMR Evidence for Finite-Size Skyrmions in GaAs Quantum Wells Near Landau Level Filling $\nu = 1$, *Phys. Rev. Lett.* **74**, 5112 (1995).
- [39] M. Gradhand, D. V. Fedorov, F. Pientka, P. Zahn, I. Mertig, and B. L. Györfy, First-principle calculations of the Berry curvature of Bloch states for charge and spin transport of electrons, *J. Phys.: Condens. Matter* **24**, 213202 (2012).
- [40] T. Fukui, Y. Hatsugai, and H. Suzuki, Chern numbers in discretized Brillouin zone: Efficient method of computing (spin) Hall conductances, *J. Phys. Soc. Jpn.* **74**, 1674 (2005).
- [41] S. Deng, L. Viola, and G. Ortiz, Majorana Modes in Time-Reversal Invariant s -Wave Topological Superconductors, *Phys. Rev. Lett.* **108**, 036803 (2012).

- [42] N. Nagaosa, J. Sinova, S. Onoda, A. H. MacDonald, and N. P. Ong, Anomalous Hall effect, *Rev. Mod. Phys.* **82**, 1539 (2010).
- [43] H. Bruus and K. Flensberg, *Many-Body Quantum Theory in Condensed Matter Physics* (Oxford University Press, New York, 2004).
- [44] K. Moon, H. Mori, K. Yang, S. M. Girvin, A. H. MacDonald, L. Zheng, D. Yoshioka, and S.-C. Zhang, Spontaneous interlayer coherence in double-layer quantum Hall systems: Charged vortices and Kosterlitz-Thouless phase transitions, *Phys. Rev. B* **51**, 5138 (1995).
- [45] K. Nomura and A. H. MacDonald, Quantum Hall Ferromagnetism in Graphene, *Phys. Rev. Lett.* **96**, 256602 (2006).
- [46] J. Alicea and M. P. A. Fisher, Graphene integer quantum Hall effect in the ferromagnetic and paramagnetic regimes, *Phys. Rev. B* **74**, 075422 (2006).
- [47] K. Yang, S. Das Sarma, and A. H. MacDonald, Collective modes and skyrmion excitations in graphene $SU(4)$ quantum Hall ferromagnets, *Phys. Rev. B* **74**, 075423 (2006).
- [48] M. Kharitonov, Phase diagram for the $\nu = 0$ quantum Hall state in monolayer graphene, *Phys. Rev. B* **85**, 155439 (2012).
- [49] M. Kharitonov, Edge excitations of the canted antiferromagnetic phase of the $\nu = 0$ quantum Hall state in graphene: A simplified analysis, *Phys. Rev. B* **86**, 075450 (2012).
- [50] A. F. Young, J. D. Sanchez-Yamagishi, B. Hunt, S. H. Choi, K. Watanabe, T. Taniguchi, R. C. Ashoori, and P. Jarillo-Herrero, Tunable symmetry breaking and helical edge transport in a graphene quantum spin Hall state, *Nature (London)* **505**, 528 (2013).
- [51] N. B. Kopnin, T. T. Heikkilä, and G. E. Volovik, High-temperature surface superconductivity in topological flat-band systems, *Phys. Rev. B* **83**, 220503(R) (2011).
- [52] B. Pamuk, J. Baima, F. Mauri, and M. Calandra, Magnetic gap opening in rhombohedral-stacked multilayer graphene from first principles, *Phys. Rev. B* **95**, 075422 (2017).
- [53] T. Löthman and A. M. Black-Schaffer, Universal phase diagrams with superconducting domes for electronic flat bands, *Phys. Rev. B* **96**, 064505 (2017).
- [54] Y. Cao, V. Fatemi, S. Fang, K. Watanabe, T. Taniguchi, E. Kaxiras, and P. Jarillo-Herrero, Unconventional superconductivity in magic-angle graphene superlattices, *Nature (London)* **556**, 43 (2018).
- [55] Y. Cao, V. Fatemi, A. Demir, S. Fang, S. L. Tomarken, J. Y. Luo, J. D. Sanchez-Yamagishi, K. Watanabe, T. Taniguchi, E. Kaxiras, R. C. Ashoori, and P. Jarillo-Herrero, Correlated insulator behavior at half-filling in magic-angle graphene superlattices, *Nature (London)* **556**, 80 (2018).
- [56] A. L. Sharpe, E. J. Fox, A. W. Barnard, J. Finney, K. Watanabe, T. Taniguchi, M. A. Kastner, and D. Goldhaber-Gordon, Emergent ferromagnetism near three-quarters filling in twisted bilayer graphene, *Science* **365**, 605 (2019).
- [57] X. Lu, P. Stepanov, W. Yang, M. Xie, M. A. Aamir, I. Das, C. Urgell, K. Watanabe, T. Taniguchi, G. Zhang, A. Bachtold, A. H. MacDonald, and D. K. Efetov, Superconductors, orbital magnets, and correlated states in magic angle bilayer graphene, [arXiv:1903.06513](https://arxiv.org/abs/1903.06513).
- [58] X. Liu, Z. Hao, E. Khalaf, J. Y. Lee, K. Watanabe, T. Taniguchi, A. Vishwanath, and P. Kim, Spin-polarized correlated insulator and superconductor in twisted double bilayer graphene, [arXiv:1903.08130](https://arxiv.org/abs/1903.08130).
- [59] A. V. Balatsky, I. Vekhter, and J.-X. Zhu, Impurity-induced states in conventional and unconventional superconductors, *Rev. Mod. Phys.* **78**, 373 (2006).
- [60] H. Alloul, J. Bobroff, M. Gabay, and P. J. Hirschfeld, Defects in correlated metals and superconductors, *Rev. Mod. Phys.* **81**, 45 (2009).
- [61] A. P. Mackenzie, R. K. W. Haselwimmer, A. W. Tyler, G. G. Lonzarich, Y. Mori, S. Nishizaki, and Y. Maeno, Extremely Strong Dependence of Superconductivity on Disorder in Sr_2RuO_4 , *Phys. Rev. Lett.* **80**, 161 (1998).